ACS OMEGA



http://pubs.acs.org/journal/acsodf
Article

# Determination of the Catalytic Activity of a Peroxidase-like Nanozyme and Differences among Layered Double Hydroxides with Different Anions and Cations

MingZe Ma, Hai Wang, TieYing Zhang, XueJing Wang, ZhiHua Xu, RenYin Zhang, XiaoYu Ma, and Feng Shi*

Cite This: *ACS Omega* 2023, 8, 35779−35790

Read Online

ACCESS | Metrics & More | Article Recommendations | Supporting Information

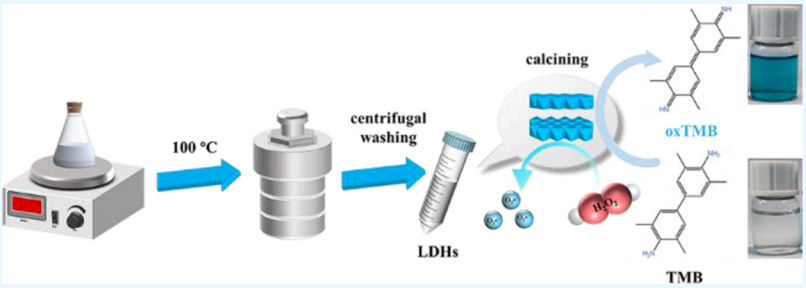


**ABSTRACT:** Nanomaterials with enzyme-like activity, namely, nanozymes, have been widely used as substitutes for natural enzymes, and they show excellent potential for application in many fields, such as biotechnology, environmental chemistry, and medicine. Layered double hydroxides (LDHs) are inorganic nanomaterials with adjustable compositions, simple preparation methods, and low costs and are some of the most promising candidate materials for the preparation of nanozymes. Here, we studied the syntheses and peroxidase-like activities of LDHs with four anions and four cations. First, LDHs prepared by the coprecipitation-hydrothermal method adopted hexagonal lamellar structures with good dispersion and uniform particle sizes. The Lambert−Beer law showed that the prepared LDHs exhibited good enzymatic activity. Later, the $K_m$ and $V_{max}$ values of the LDHs with different anionic/cationic materials intercalated into their structures were compared. Under the optimum conditions, the $V_{max}$ of $Mg_2Al$-$NO_3$-LDH was $7.35 \times 10^{-2}$, which is 2−4 times higher than that of the LDHs containing other anions; the $V_{max}$ values of NiFe-LDH and FeAl-LDH were 0.152 and 0.284, respectively, which are 10 times higher than those of the LDHs with other cations. Importantly, according to kinetic analyses of the enzymatic reactions, the effects of $Fe^{2+}$ and $Fe^{3+}$ on the LDH enzyme activity were greater than those of the intercalated anions. This study showed that NiFe-LDH and FeAl-LDH with high catalytic activities are candidate materials for peroxidase simulations, which may provide new strategies for the application of LDHs in biosensors, antioxidants, biotechnology, and other nanozyme applications.

## 1. INTRODUCTION

Enzymes are biomacromolecules that can catalyze and, thus, accelerate biochemical reactions under mild conditions. They play important roles in biological reactions. However, since most enzymes are proteins, they have poor molecular stabilities, are sensitive to the environment, are easy to degrade or inactivate, require complex preparation and purification processes, and have high costs, and these factors greatly limit the large-scale production and application of biological enzymes.[1] Therefore, nanozymes composed of inorganic materials have attracted increasing attention from scientists. In 2007, Yan discovered that magnetic iron oxide nanoparticles ($Fe_3O_4$ MNPs) showed enzymatic activity with a mechanism of action similar to that of horseradish peroxidase (HRP).[2] In 2013, Wei summarized various strategies for modulating the activity and selectivity of nanozymes.[3] Since then, the field of nanozymes has made rapid progress. In the past decade, more than 300 nanomaterials have been reported to have intrinsic enzyme-like activity.[4] Compared with natural enzymes that are easily inactivated in extreme environments, nanozymes have catalytic efficiencies similar to those of natural enzymes and the advantages of greater stability, lower cost, and easier preparation than natural enzymes. Based on the material type, nanozymes can be roughly divided into three categories: metal-based nanozymes (e.g., gold, platinum, and cobalt), metal oxide or metal sulfide nanozymes (e.g., ferric oxide and

Received: May 11, 2023
Accepted: September 13, 2023
Published: September 22, 2023

iron sulfide), and carbon-based nanozymes (e.g., graphene and carbon dots).[5]

In recent years, various structure−activity relationships of peroxidases have been reported. Gao et al. showed that the catalytic activity of $Fe_3O_4$ nanoparticles with peroxidase-like activity was pH-, temperature-, and $H_2O_2$ concentration-dependent and proposed a Fenton-like mechanism to explain this activity.[2] Tian et al. found that the peroxidase activity of $CeO_2$ was related to its morphology.[6] Dong et al. compared the peroxidase activity of $Ce_3O_4$ with that of $Fe_3O_4$ and proposed an electron-transfer mechanism, which provided a quantitative understanding of the peroxidase activity.[7] Shen et al. generated a volcano plot of peroxidase-like activity, which can be used to predict the catalytic activities of material surfaces.[8] Despite progress, there are still some difficulties in characterizing the microscale mechanism and kinetics of peroxidase activity.

Layered double hydroxides (LDHs), also known as intercalated hydrotalcite or hydrotalcite-like materials, are compounds formed by the orderly assembly of interlayer anions and positively charged laminates. Their structures are similar to that of brucite $Mg(OH)_2$, which comprises $MO_6$ octahedra with shared edges (Figure 1). LDHs have the general formula $M^{2+}{}_{1-x}M^{3+}{}_x(OH)_2]^{x+}(A^{n-})_{x/n}\cdot mH_2O$, where $M^{2+}$ and $M^{3+}$ are divalent and trivalent metal cations, respectively, located on the main laminate. $A^{n-}$ is an interlayer anion, $x$ is the molar ratio of $M^{3+}$/ ($M^{2+}$+ $M^{3+}$), and $m$ is the number of interlayer water molecules.[9,10]

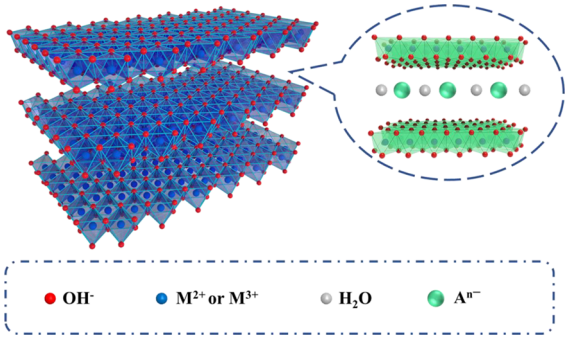


**Figure 1.** Structure of LDH ($[M^{2+}{}_{1-x}M^{3+}{}_x(OH)_2]^{x+}(A^{n-})_{x/n}\cdot mH_2O$); the right figure shows the enlarged interlayer structure of LDH.

LDH laminates are formed with strong chemical bonds, and the layers are bonded by weak electrostatic forces and hydrogen bonds; thus, the interlayer anions are easily exchanged with other anions that are more easily inserted into the layers.[11,12] For common inorganic anions, the order of anion exchange capacity in LDHs decreases in the order $CO_3^{2-}$ > $SO_4^{2-}$ > $OH^-$ > $Cl^-$ > $NO_3^-$.[13] As long as the ionic radii of the $M^{2+}$ and $M^{3+}$ metal cations are not very different from that of $Mg^{2+}$, they can covalently bond with hydroxyl groups to form layered structures similar to that of $Mg(OH)_2$. LDHs have many advantageous chemical and physical properties, such as high stability, catalytic ability, high specific surface area, nontoxicity, and anion exchange capacity.[14] Because of these properties, LDHs are widely used in different applications, such as adsorbents, catalysis, and biomedicine.[15−18]

Additionally, many studies have shown that LDHs have the advantages of high specific surface areas, ample redox reaction active centers, controllable morphologies and sizes, and biocompatibility, and they are attractive enzyme mimics.[14] In this study, four kinds of LDHs with different cations and four kinds of Mg−Al-LDH anions were prepared via a coprecipitation-hydrothermal method. The aim was to standardize the determination of the catalytic activities and kinetics of the peroxidase-like nanozymes. The catalytic activities and enzymatic reaction kinetics of the eight prepared LDHs were compared, providing a theoretical basis for biological applications of LDH nanozymes.

## 2. MATERIALS AND METHODS

**2.1. Reagents.** 3,3′,5,5′-Tetramethylbenzidine (TMB) (molecular weight: 240.35, purity ≥99%) was obtained from Beijing Balinway Technology Co., Ltd. Sodium hydroxide (NaOH), iron(II) chloride tetrahydrate ($FeCl_2\cdot 4H_2O$), iron nitrate nonahydrate ($Fe(NO_3)_3\cdot 9H_2O$), anhydrous sodium carbonate ($Na_2CO_3$) (molecular weight: 105.99, purity ≥98%), and anhydrous sodium sulfate ($Na_2SO_4$) (molecular weight: 142.04, purity ≥98%) were purchased from Shanghai Macklin Biochemical Technology Co., Ltd. Magnesium nitrate hexahydrate ($Mg(NO_3)_2\cdot 6H_2O$), cobalt chloride hexahydrate ($CoCl_2\cdot 6H_2O$), aluminum nitrate nonahydrate ($Al(NO_3)_3\cdot 9H_2O$), nickel nitrate hexahydrate ($Ni(NO_3)_2\cdot 6H_2O$), magnesium chloride hexahydrate ($MgCl_2\cdot 6H_2O$), and aluminum chloride hexahydrate ($AlCl_3\cdot 6H_2O$) were purchased from Sigma (St. Louis, MO, USA). All other chemical reagents were of analytical grade. All experiments were performed using ultrapure water from a Milli-Q A10 water purification system.

**2.2. LDH Synthesis.** LDHs with four different cations and four different $Mg_2$-Al-LDH anions were prepared by coprecipitation and subsequent hydrothermal treatment.

*2.2.1. Preparation of LDHs with Different Anions.* As mentioned above, $Mg_2$-Al-LDHs containing $Cl^-$, $CO_3^{2-}$, $NO_3^-$, or $SO_4^{2-}$ as the interlayer anion were prepared by a coprecipitation-hydrothermal method at room temperature.[19,20] Briefly, salt solution A containing $MgCl_2$ (2.0 mmol) and $AlCl_3$ (1.0 mmol) and solution B containing 40 mL of NaOH (0.15 M) were mixed with vigorous stirring under a $N_2$ atmosphere, and the resulting precipitate was washed twice at 6000 rpm for 10 min, dispersed in 40 mL of water, and then hydrothermally treated in an autoclave (Teflon inner liner) at 100 °C for 16 h to obtain a $Mg_2$Al-Cl-LDH suspension with a mass concentration of 4.0 mg/mL. When 0.013 M anhydrous $Na_2CO_3$ or 0.013 M anhydrous $Na_2SO_4$ was added to solution B, $Mg_2$Al-$CO_3$-LDH with a mass concentration of 6.0 mg/mL or a $Mg_2$Al-$SO_4$-LDH suspension with a mass concentration of 3.0 mg/mL was obtained.

$Mg_2$Al-$NO_3$-LDH nanosheets were prepared via an improved nonaqueous precipitation method.[21,22] First, 10 mL of methanol solution containing $Mg(NO_3)_2\cdot 6H_2O$, $Al(NO_3)_3\cdot 9H_2O$ (2.0 mmol), and $AlCl_3$ (1.0 mmol) was mixed under vigorous stirring and added dropwise to 40 mL of methanol solution containing NaOH (0.15 M), and the mixture was stirred for 30−40 min in a $N_2$ atmosphere. The precipitate slurry was then collected through centrifugation, redispersed in fresh methanol (40 mL), and transferred to an autoclave (Teflon inner liner), where it was heated to 100 °C for 18 h and then cooled to room temperature. The precipitate was collected by centrifugation at 5000 rpm, washed twice with deionized water, and dispersed in 40 mL of deionized water, resulting in a homogeneous suspension of 8.0 mg/mL $Mg_2$Al-$NO_3$-LDH after 4−6 days. It is to be noted that due to the strong intercalation ability of $CO_3^{2-}$, $N_2$ purging was required in the preparation of $Mg_2$Al-Cl-LDH, $Mg_2$Al-$NO_3$-LDH, and


https://doi.org/10.1021/acsomega.3c03287
ACS Omega 2023, 8, 35779−35790

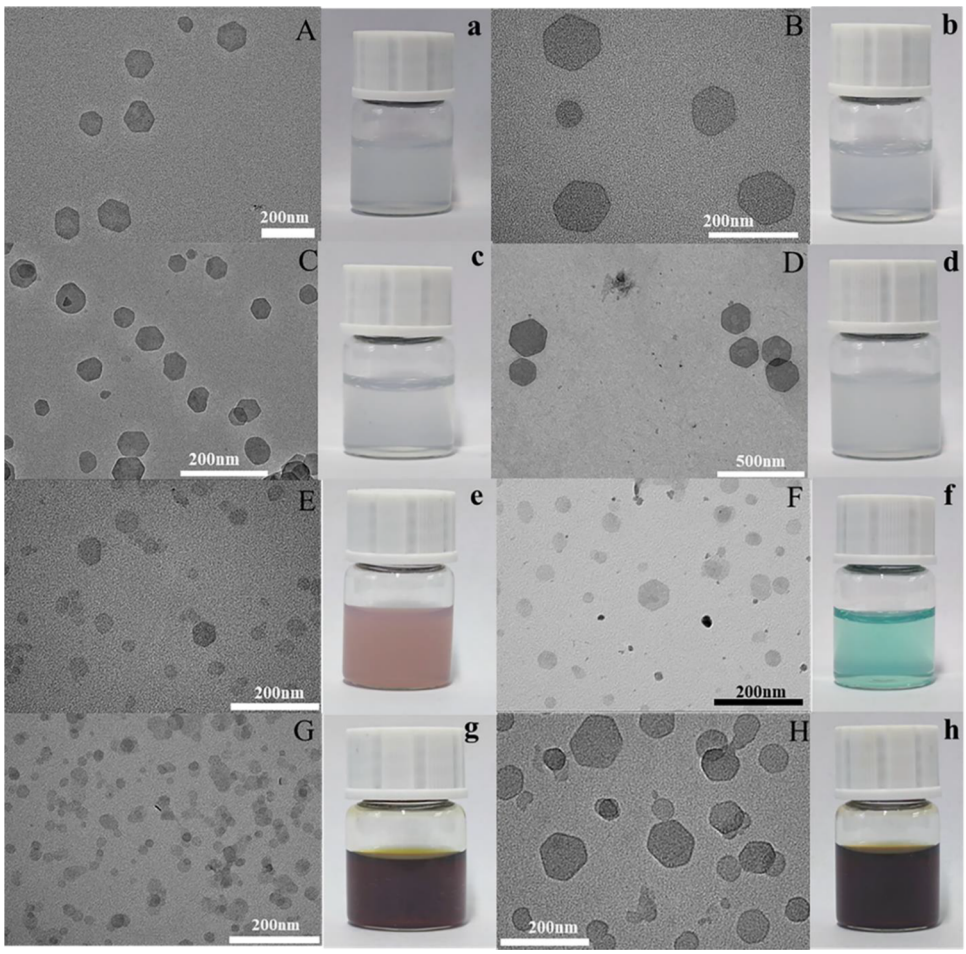


**Figure 2.** TEM images of LDHs with different anions and cations [$Mg_2Al$-Cl-LDH (A), $Mg_2Al$-$CO_3$-LDH (B), $Mg_2Al$-$NO_3$-LDH (C), $Mg_2Al$-$SO_4$-LDH (D), $Co_2Al$-LDH (E), $Ni_2Al$-LDH (F), $Ni_2Fe$-LDH (G), and $Fe_2Al$-LDH (H); a, b, c, d, e, f, g, and h show the corresponding suspensions dispersed in ultrapure water].

$Mg_2Al$-$SO_4$-LDH to eliminate the interference of $CO_2$ dissolution in air.

*2.2.2. Preparation of Cationic LDHs.* Salt solution A containing $CoCl_2$ (2.0 mmol) and $AlCl_3$ (1.0 mmol) and mixed solution B containing 20 mL of NaOH (0.15 M) and anhydrous $Na_2CO_3$ (0.013 M) were stirred vigorously, and the LDH was collected by centrifugation and then washed twice with deionized water. Then, the suspension solution was treated in an autoclave (Teflon inner liner) at 100 °C for 16 h to obtain CoAl-LDH with a mass concentration of 5.0 mg/mL.[23] When salt solution A contained $FeCl_2$ (2.0 mmol) and $AlCl_3$ (1.0 mmol), $Ni(NO_3)_2{\cdot}6H_2O$ (3.6 mmol) and $Fe(NO_3)_3{\cdot}9H_2O$ (1.2 mmol) or $Ni(NO_3)_2{\cdot}6H_2O$ (3.6 mmol), and $Al(NO_3)_3$ (1.2 mmol), an FeAl-LDH suspension with a mass concentration of 4.0 mg/mL,[24] a NiFe-LDH suspension with a mass concentration of 12.0 mg/mL[25] or a NiAl-LDH suspension with a mass concentration of 11.0 mg/mL was obtained.[26]

**2.3. Characterization.** Parameters such as the properties, morphologies, particle sizes, and dispersions of the LDHs were determined via enzyme labeling analysis, particle size analysis (Malvern instrument), Fourier transform infrared (FT-IR) spectroscopy, transmission electron microscopy (TEM), and X-ray powder diffraction (XRD).

The particle size distributions, molecular weights, and zeta potentials of the LDHs were measured with a Malvern particle size analyzer to characterize the mean particle size, particle size distribution, and stability of the colloidal dispersion system.

The samples were prepared by drip coating a colloidal solution of LDHs (5 mL) onto a hydrophilic copper grid. After the samples were dried at room temperature, the mean particle size, surface morphology, and dispersion of the as-prepared LDHs were determined via TEM (Hitachi HT7700).

The prepared LDHs were centrifuged at 10,000 rpm for 30 min, and the precipitate was ground into a fine powder, which was evenly mixed with dried KBr and pressed into thin pellets. Then, FT-IR spectra were recorded on a Nicolet 6700 spectrometer from 400 to 4000 $cm^{-1}$.

XRD patterns for the LDHs were obtained with a D8 ADVANCE X-ray diffractometer. The scan rate was 6.00°/min, and the range was 5−90°.

**2.4. Study of the Optimum Conditions for LDH Enzyme Activity.** Five micrograms of nanozyme was added to 96-well plates with 0.2 M NaAc−HAc buffer with different pH values (2.0, 2.4, 2.8, 3.2, 3.6, 4.0, 4.4, 5.2, 5.6, 6.4, 7.2, 8.0, 8.8, 9.6, 10.4, 11.2). The amount of the chromogenic agent TMB (10 $mg{\cdot}mL^{-1}$) added was 10 $\mu$L. The reaction mixture was placed in a constant-temperature water bath and incubated in the dark at room temperature for 1 min. $H_2O_2$ (30%) was added to achieve a final concentration of 1 M. After 5 min of reaction, the absorbance was measured at 652 nm by using a microplate reader.


https://doi.org/10.1021/acsomega.3c03287
ACS Omega 2023, 8, 35779−35790

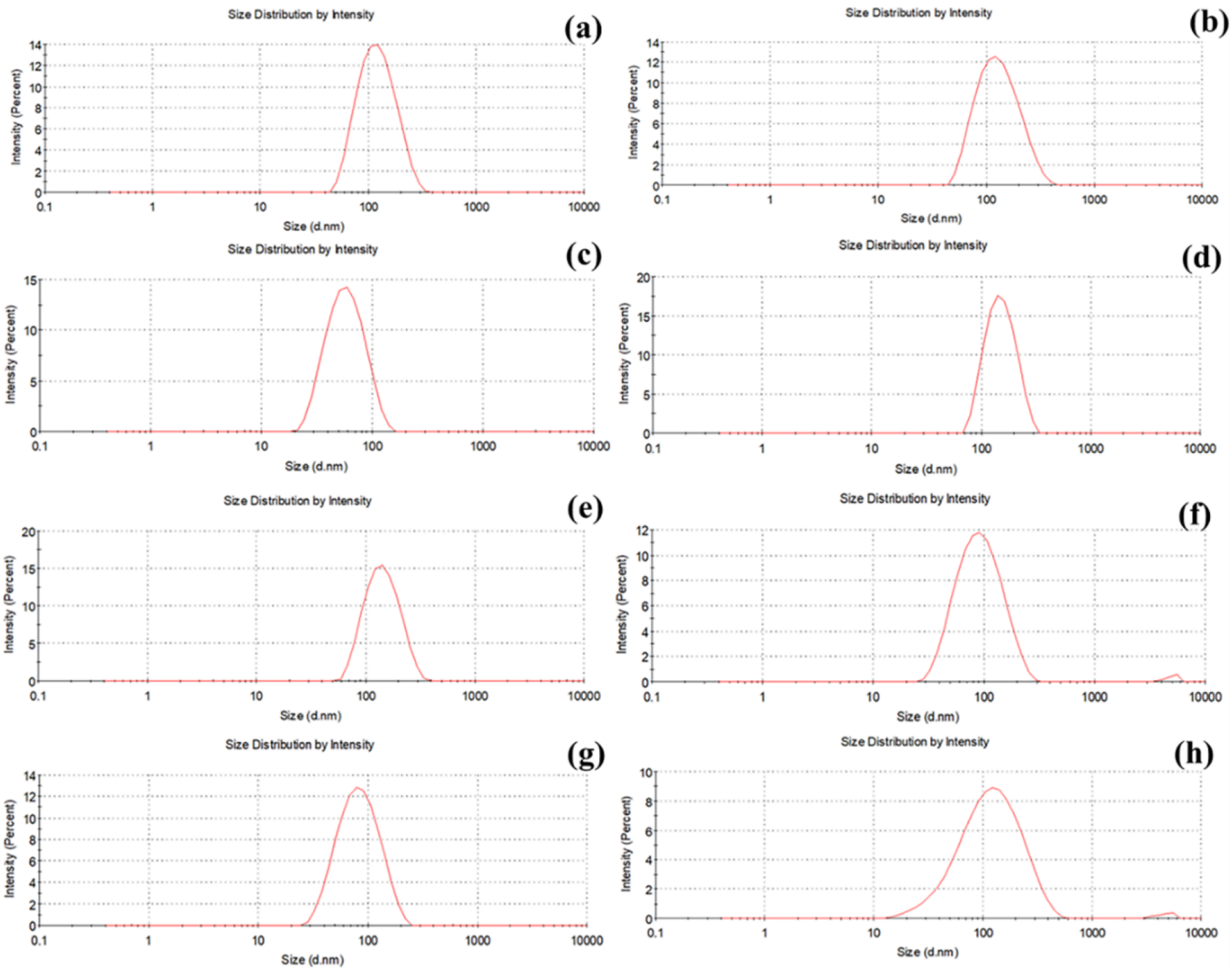


**Figure 3.** Particle size distributions of LDHs with different anions and cations [$Mg_2Al$-Cl-LDH (a), $Mg_2Al$-$CO_3$-LDH (b), $Mg_2Al$-$NO_3$-LDH (c), $Mg_2Al$-$SO_4$-LDH (d), CoAl-LDH (e), NiAl-LDH (f), NiFe-LDH (g), and FeAl-LDH (h)].

The nanozyme (5 $\mu$g) was added to 96-well plates containing 0.2 M NaAc−HAc buffer at the same pH (optimum pH). The amount of the chromogenic agent TMB (10 mg·mL$^{-1}$) added was 10 $\mu$L. The reaction mixture was placed in a constant-temperature water bath and incubated in the dark at room temperature for 1 min. The mixture was placed into a water bath pot with a temperature gradient of 20, 25, 30, 35, 40, 45, 50, 55, and 60 °C. $H_2O_2$ (30%) was added to achieve a final concentration of 1 M. After 5 min of reaction, the absorbance was measured at 652 nm using a microplate reader.

**2.5. Determination of the Peroxidase-like Activities of LDHs.** Fifty micrograms of LDH was added to a cuvette containing 0.2 M NaAc−HAc buffer at the same pH (optimum pH). The amount of the chromogenic agent TMB (10 mg·mL$^{-1}$) added was 100 $\mu$L. The reaction mixture was placed in a constant-temperature water bath and incubated at a specific temperature (optimum temperature) for 1 min under dark conditions. $H_2O_2$ (30%) was added to achieve a final concentration of 1 M. In addition to the prepared sample, a sample without a $H_2O_2$ solution was prepared as a reference solution for the measurements. The samples were mixed and reacted under the optimum conditions of darkness. After addition of $H_2O_2$, the absorbance at 652 nm, reflecting the colorimetric value, was recorded for up to 300 s. The optical density (OD) at 652 nm versus time was plotted, and the nanozyme activity unit ($U$) and specific activity (SA) were calculated by means of the following formula.

$$U_{\text{nanozyme}} = V/(\varepsilon \times l) \times \Delta A/\Delta t$$

$U_{\text{nanozyme}}$ indicates the catalytic activity of the nanozymes ($\mu$mol·min$^{-1}$), $V$ is the total volume of the reaction solution ($\mu$L), $\varepsilon$ is the molar absorption coefficient of TMB at 652 nm (39,000 M$^{-1}$·cm$^{-1}$), $l$ is the length of light transmission (cm), and $A$ is the absorbance value obtained after subtracting that of the blank reference. $\Delta A/\Delta t$ is the initial change rate of the OD value and time relationship curve at 652 nm for 1 min.

$$\text{SA}_{\text{nanozyme}} = U_{\text{nanozyme}}/[m]$$

SA is the unit of activity per milligram of nanozyme (U·mg$^{-1}$) and $[m]$ is the weight of nanozymes for the reaction (mg).

## 3. RESULTS AND DISCUSSION

**3.1. Synthesis and Characterization of the LDHs.** To characterize the shapes, dimensions, and size distributions of the LDHs, TEM measurements were performed. The TEM


https://doi.org/10.1021/acsomega.3c03287
ACS Omega 2023, 8, 35779−35790

images of the LDHs synthesized in this study are shown in Figure 2. The nanoparticles were in the form of hexagonal nanosheets, and the lateral sizes of most sheets were 40−160 nm. The average particle size of the MgAl-LDH samples was in the range 150−50 nm, with a smaller value for the nitrate-containing sample synthesized in methanol. Among the sampes, $Mg_2Al$-$NO_3$-LDH had the smallest particle size of 50 ± 15 nm, while $Mg_2Al$-Cl-LDH, $Mg_2Al$-$CO_3$-LDH, and $Mg_2Al$-$SO_4$-LDH had particle sizes of 130 ± 30 nm. Depending on the nature of the cation, the average particle size varied from 132 to 74 nm, with smaller values observed for the Ni-containing samples. The particle sizes of NiAl and NiFe were 50 ± 30 nm, and the particle sizes of CoAl and FeAl were 110 ± 30 nm. Thus, the TEM images showed that LDHs with different anions and cations all formed hexagonal nanosheets with relatively uniform particle sizes, good dispersion, and little agglomeration, indicating the moderate stability of the prepared LDHs. This is largely consistent with the results of previous studies.[21,26−29]

The particle size analysis results for LDH samples with different anions and cations are shown in Figure 3. The figure shows that the size distribution of the LDHs in aqueous solution was relatively concentrated, and the particle size of the LDHs was between 50 and 130 nm. Among the samples, FeAl-LDHs had a wide particle size distribution and general dispersibility, and the polydispersity index (PDI) was 0.269, while the other LDHs had a narrow particle size distribution and good dispersibility. The zeta potential results can provide information about the surface charge and stability of LDHs, and the zeta potential is an important parameter for characterizing the stability of colloidal dispersion systems and predicting the long-term stability of nanoparticles.[30] The zeta potential of a sample determines whether the particles in the liquid are stable or tend to flocculate and stick together. If the absolute value of the zeta potential is large, that is, the particles have more charges, the particles repel each other so that the whole system remains stable.[31] In general, the greater the absolute value of the zeta potential is, the higher the stability of the system.[32] The zeta potential results showed that the surface charges of the eight LDHs synthesized in this study were all positive (Table 1), indicating that the nanoparticle suspension showed high stability and its electropositivity mainly originated from the positively charged lamellae of the LDHs. $Ni_2Al$-LDH and $Ni_2Fe$-LDH exhibited very different crystallinities, which, despite the similar average particle size measured by TEM, was consistent with the lower PDI of the latter. In addition, higher crystallinities were observed for $Mg_2Al$-$SO_4$-LDH, $Co_2Al$-LDH, and $Mg_2Al$-$CO_3$-LDH, consistent with their larger average particle sizes.

**Table 1. Average Particle Sizes, PDIs, and Zeta Potentials of the LDHs with Different Anions and Cations**

| LDHs | average particle size (nm) | PDI | zeta potential (mV) |
|---|---|---|---|
| MgAl-$Cl^-$ | 110.0 | 0.125 | +43.2 |
| MgAl-$CO_3^{2-}$ | 119.0 | 0.173 | +36.1 |
| MgAl-$NO_3^-$ | 51.3 | 0.230 | +42.7 |
| MgAl-$SO_4^{2-}$ | 152.5 | 0.209 | +33.8 |
| CoAl | 131.6 | 0.114 | +42.2 |
| NiAl | 79.7 | 0.245 | +45.5 |
| NiFe | 74.1 | 0.155 | +34.1 |
| FeAl | 99.0 | 0.269 | +46.0 |

The layered structures of the prepared LDH nanoparticles were confirmed by FT-IR (Figure 4) and XRD (Figure 5) studies. The FT-IR spectra of the samples are shown in Figure 4. As expected, the FT-IR spectra of the eight LDHs were essentially identical to those of conventional LDHs,[33] all of which have broad bands at approximately 3478 $cm^{-1}$ (tensile vibration of −OH in the brucite-like layer and interlayer $H_2O$ molecules), broad bands at approximately 1372 $cm^{-1}$ (bending vibrations of interlayer and adsorbed $H_2O$ molecules),[23] and absorption bands near 1350 $cm^{-1}$ attributed to the stretching vibrations of $CO_3^{2-}$, which resulted from the absorption of $CO_2$ from the air by brucite. In the spectra of $Mg_2Al$-Cl-LDH, $Mg_2Al$-$CO_3$-LDH, $Mg_2Al$-$NO_3$-LDH, and $Mg_2Al$-$SO_4$-LDH, the two weak bands near 2910 $cm^{-1}$ may be due to hydrogen bond (−OH) stretching vibrations of the intercalated water molecules. In the spectra of CoAl-LDH and NiFe-LDH, the band below 800 $cm^{-1}$ was attributed to metal−oxygen (M−O) and metal−oxygen−hydrogen (M−O−H) stretching vibrations.[21] The 1100 $cm^{-1}$ band in the spectrum of $Mg_2Al$-$SO_4$-LDH was attributed to the S−O vibration in the $SO_4^{2-}$ ions. Of particular note,[19] the bands in the spectra of $Mg_2Al$-$NO_3$-LDH, NiAl-LDH, and NiFe-LDH at approximately 1382 $cm^{-1}$ and the stretching vibration for $NO_3^-$ overlapped with the stretching vibration of $CO_3^{2-}$.[33,34] This was likely caused by the absorption of $CO_2$ from the air during preparation and drying.

The crystal structures of the eight LDHs were studied by XRD. As depicted in Figure 5a, the diffraction peaks observed at 2$\theta$ values of approximately 11.7°, 23.4°, 34.5°, 35.5°, 38.9°, 39.1°, 60.7°, and 62.1° were attributed to the (003), (006), (009), (012), (015), (018), (110), and (113) planes of the $\alpha$-$Mg(OH)_2$ phase. The (003) $d$ spacings of the prepared $Mg_2Al$-Cl-LDH, $Mg_2Al$-$CO_3$-LDH, $Mg_2Al$-$NO_3$-LDH, and $Mg_2Al$-$SO_4$-LDH samples were 0.77 0.76, 0.79, and 0.76 nm, respectively. The full widths at half-maximum (fwhm's) for the (003) reflections were 0.4°, 0.5°, 0.7°, and 0.3°. Figure 5b shows that the LDH nanoparticles with four different cations had typical layered structures, and their diffraction peaks were observed at 2$\theta$ values of 10.6° (003) and 21.7° (006). This indicated the formation of CoAl-LDH, NiAl-LDH, NiFe-LDH, and FeAl-LDH, and their (003) $d$ spacings were 0.76 0.79, 0.80, and 0.85 nm, respectively. The fwhm values of the (003) reflection were 0.3°, 1.1°, 0.8°, and 1.5°. The sharp diffraction peaks in Figure 5 show the high crystallinity and layered characteristics of the LDHs.[26]

**3.2. Optimum Conditions for LDH Peroxidase-like Activity.** The peroxidase-like activities of the prepared LDHs were studied by using TMB as a chromogenic substrate. As shown in Figure 6a, in the presence of $H_2O_2$, the LDHs promoted the oxidation of TMB. This oxidation occurred because the nanozymes catalyzed the conversion of $H_2O_2$ in the system to $O_2^{\cdot-}$, which oxidized TMB to form the typical blue product (OxTMB) with an absorption peak at 652 nm.[35,36]

Similar to those of other nanozymes, the catalytic efficiencies of the LDHs depended on the pH and temperature, as well as the $H_2O_2$ concentration. Using 0.2 M acetate buffer as the reaction medium, we measured the peroxidase-like activities of LDHs at pH values ranging from 2.0 to 11.2 and temperatures from 25 to 60 °C and compared the activities of the eight LDHs with different anions and cations in the same parameter range (Table 2 and Figure 7). Therefore, we used the optimum pH and temperature as the standard conditions for subsequent


https://doi.org/10.1021/acsomega.3c03287
ACS Omega 2023, 8, 35779−35790

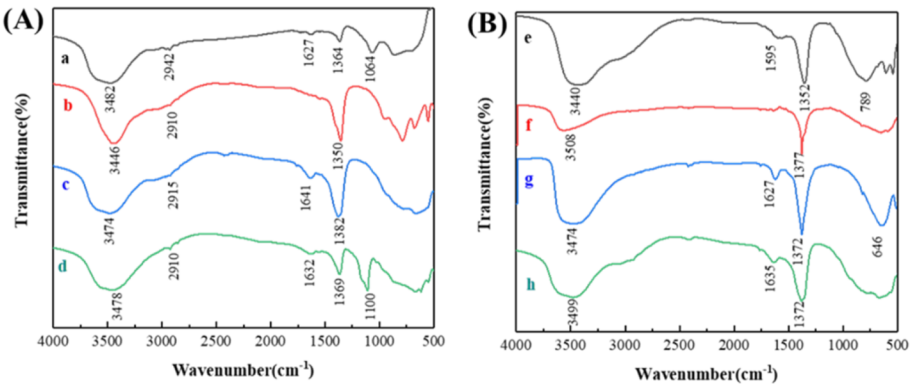


**Figure 4.** FT-IR spectra of LDHs with different anions and cations [$Mg_2Al$-Cl-LDH (a), $Mg_2Al$-$CO_3$-LDH (b), $Mg_2Al$-$NO_3$-LDH (c), $Mg_2Al$-$SO_4$-LDH (d), CoAl-LDH (e), NiAl-LDH (f), NiFe-LDH (g), and FeAl-LDH (h)].

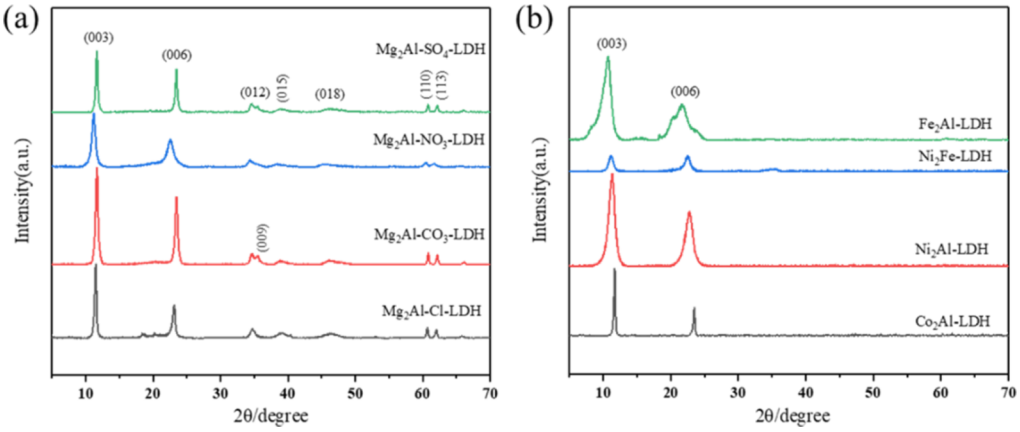


**Figure 5.** XRD patterns of the LDHs with different anions (a) and cations (b).

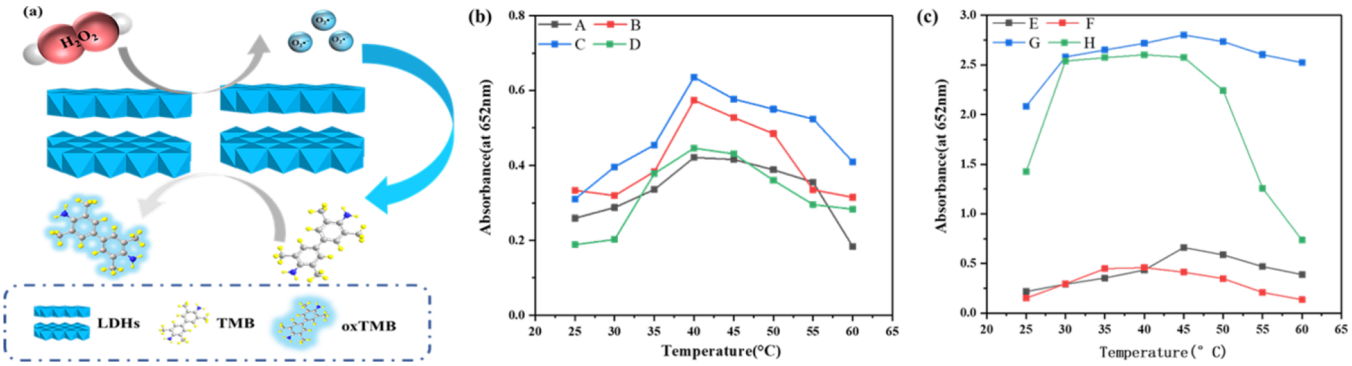


**Figure 6.** (a) Test principle used for determining the peroxidase-like activities of LDHs with $H_2O_2$ and TMB. (b) Relationships between the peroxidase-like activities of LDHs with four different anions and temperature. (c) Relationships between the peroxidase-like activity and temperature for LDHs with four different cations [$Mg_2Al$-Cl-LDHs (A), $Mg_2Al$-$CO_3$-LDHs (B), $Mg_2Al$-$NO_3$-LDHs (C), $Mg_2Al$-$SO_4$-LDHs (D), $Co_2Al$-LDHs (E), $Ni_2Al$-LDHs (F), $Ni_2Fe$-LDHs (G), and $Fe_2Al$-LDHs (H)].

**Table 2. Optimum pH and Temperature of Eight LDHs**

| LDHs | optimum temperature (°C) | optimum pH |
|---|---|---|
| MgAl-$Cl^-$ | 40 | 4.0 |
| MgAl-$CO_3^{2-}$ | 40 | 4.0 |
| MgAl-$NO_3^-$ | 40 | 4.0 |
| MgAl-$SO_4^{2-}$ | 40 | 4.0 |
| CoAl | 45 | 4.4 |
| NiAl | 40 | 4.4 |
| NiFe | 45 | 4.0 |
| FeAl | 45 | 3.6 |

analyses of the LDH activities. From a microscale point of view, the catalytic activities of nanoparticles are determined by the total number of catalytically active sites and the activity of each site.[37] The results showed that $Mg_2Al$-$NO_3$-LDH with an average particle size of 51.28 nm had a higher peroxidase-like activity under the optimal conditions than the systems containing the other three anions. This may have resulted because the smaller nanoparticles had larger active surface areas and more substrate interactions. The smaller the particle size was, the higher the catalytic activity.[2] Among the different cations, the peroxidase-like activities of NiFe-LDH and FeAl-


https://doi.org/10.1021/acsomega.3c03287
ACS Omega 2023, 8, 35779−35790

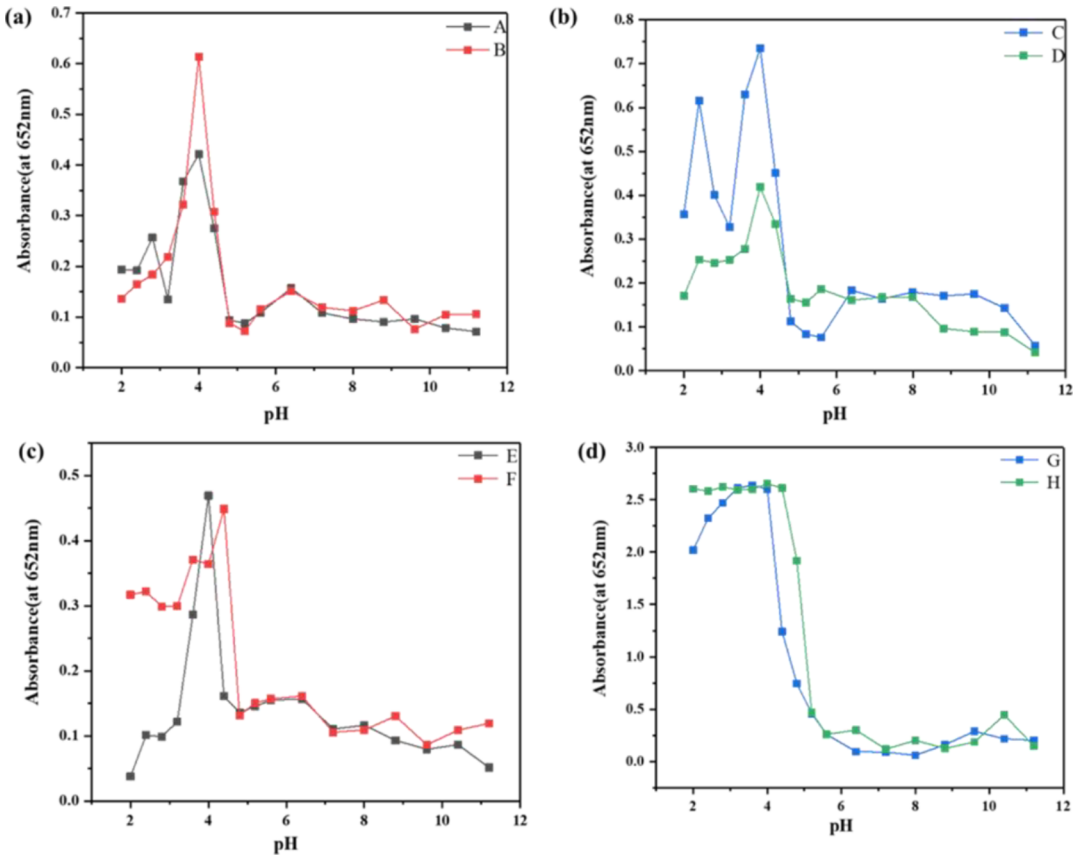


**Figure 7.** Relationships between the peroxidase-like activities of LDHs with four different anions and pH (a, b) and relationships between the peroxidase-like activities of LDHs with four different cations and temperature (c, d) [$Mg_2Al$-Cl-LDHs (A), $Mg_2Al$-$CO_3$-LDHs (B), $Mg_2Al$-$NO_3$-LDHs (C), $Mg_2Al$-$SO_4$-LDHs (D), $Co_2Al$-LDHs (E), $Ni_2Al$-LDHs (F), $Ni_2Fe$-LDHs (G), and $Fe_2Al$-LDHs (H)].

LDH under the optimal conditions were greater than those of the other two cations, which may be because $Fe^{2+}$ and $Fe^{3+}$ played major roles in the catalytic peroxidase-like activities of these LDHs. Due to the formation of cationic LDHs, the catalytic oxidation of TMB by $H_2O_2$ was much faster in acidic solution than in neutral or alkaline solutions. A possible reason is that the LDHs had sufficient positive charges in acidic solution, which ensured the stabilities of the prepared LDHs.[38]

**3.3. Peroxidase-like Activities of LDHs.** The reaction time curves for the nanozyme-catalyzed reaction of TMB were plotted at the optimum pH and temperature with 50 $\mu$g of LDH, 1650 $\mu$L of 0.2 M NaAc, 1.6 mM TMB, and 1 mM $H_2O_2$ (Figure 8a,c). Figure 8 shows the initial linear portion of the enlarged nanozyme reaction time curve. The initial period was chosen as 60 s because the $R^2$ coefficient determined by linear regression analysis was close to 1.

In addition, it was hypothesized that the observed catalytic activities of the nanozymes originated from the nanoparticles themselves and not from ions dissolved in the acidic reaction solution. To test this hypothesis, we incubated LDHs in a standard reaction solution (NaAc−HAc buffer at pH 4.0) at the optimum temperature for 300 s (the time required for the activity measurement) and then centrifuged them to remove LDH precipitates from the solution and collect the supernatant. We compared the activities of the supernatants with the activities of the collected LDHs under the same conditions (Figure 8c,f). The results showed that the leaching solution exhibited almost no catalytic activity, but the catalytic activity was observed from the collected nanoparticles. These results showed that the catalytic activity measurements (only incubation for 300 s under pH 4.0 reaction conditions) did not affect the structural integrities of the test particles (Table 3).

**3.4. Michaelis−Menten Reaction Kinetics of LDHs.** Since the catalytic activity of a nanozyme is related to the concentrations of $H_2O_2$ and TMB, the catalytic processes were studied under optimized conditions to better quantify the catalytic efficiencies of the LDHs and the effects of TMB and $H_2O_2$. The Michaelis−Menten curves were plotted for the eight materials ($Mg_2Al$-Cl-LDH, $Mg_2Al$-$CO_3$-LDH, $Mg_2Al$-$NO_3$-LDH, $Mg_2Al$-$SO_4$-LDH, CoAl-LDH, NiAl-LDH, NiFe-LDH, and FeAl-LDH). In general, peroxidase-like activity is related to the generation of free radicals. $H_2O_2$ can be adsorbed on the surfaces of LDHs, and the O−O bond of $H_2O_2$ may be cleaved to generate two $HO^{\cdot}$ radicals.[39] The generated $HO^{\cdot}$ radicals may interact with the LDHs through partial electron exchange, which may contribute to the catalytic abilities of the LDHs.[40] The peroxidase activity of LDHs may also be related to the electron-transfer mechanism. The wide bandgap between $H_2O_2$ and TMB suppresses the direct electron transfer from TMB to $H_2O_2$.[41] The reduction potential of LDHs lies exactly between that of $H_2O_2$ and that of TMB, facilitating electron transfer from TMB to $H_2O_2$ via LDHs, and the surface properties of the LDHs can affect the $H_2O_2$ absorption and particle-mediated electron-transfer processes.

Figures 9 and 10 show a typical Michaelis−Menten curve observed for an LDH within a suitable $H_2O_2$ and TMB


https://doi.org/10.1021/acsomega.3c03287
ACS Omega 2023, 8, 35779−35790

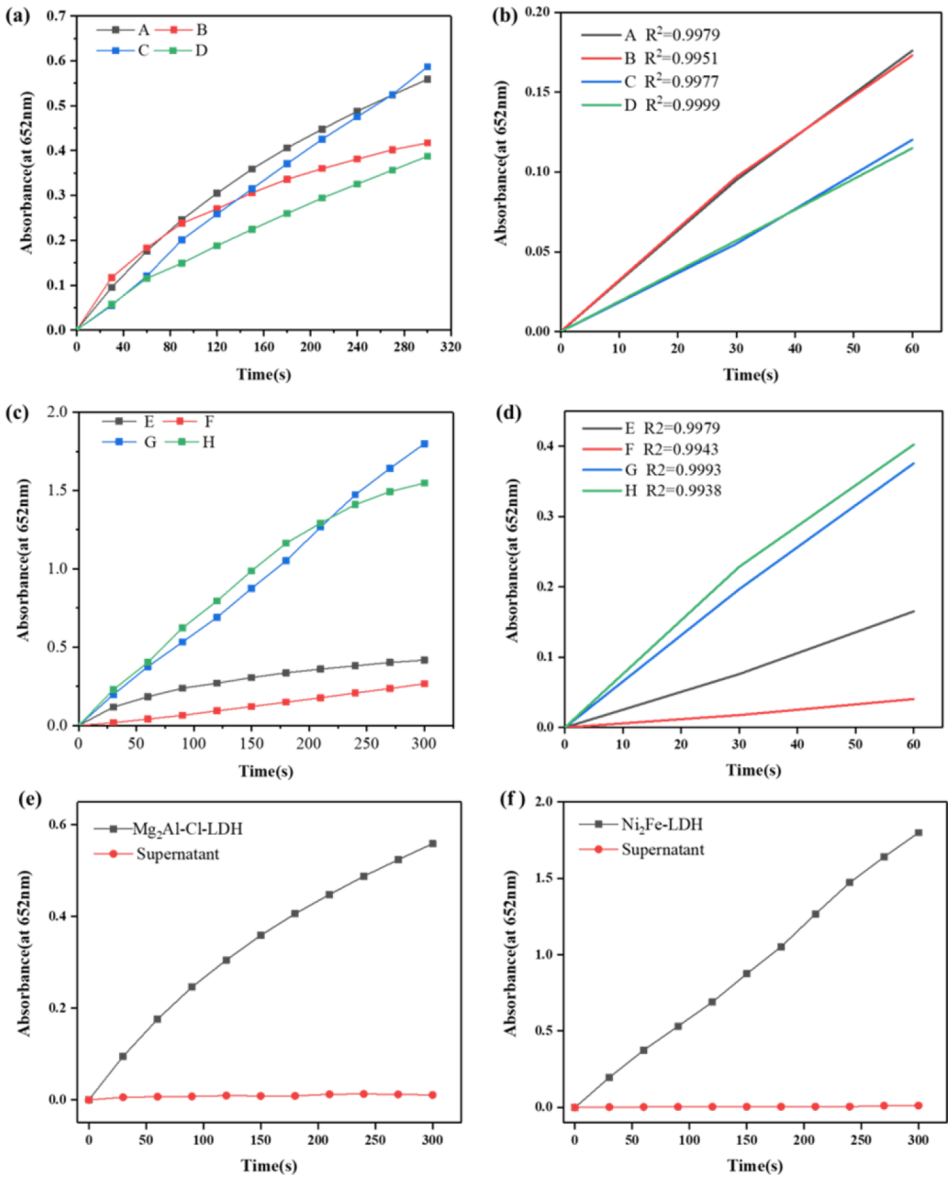


**Figure 8.** Determination of peroxidase-like activities for LDHs (a, c). The enlarged initial linear parts (b) and (d) of the nanozyme reaction time curve. Comparison of LDH activity with supernatant activity after centrifugation (e, f) [$Mg_2Al$-Cl-LDHs (A), $Mg_2Al$-$CO_3$-LDHs (B), $Mg_2Al$-$NO_3$-LDHs (C), $Mg_2Al$-$SO_4$-LDHs (D), $Co_2Al$-LDHs (E), $Ni_2Al$-LDHs (F), $Ni_2Fe$-LDHs (G), and $Fe_2Al$-LDHs (H)].

**Table 3. Results of Enzyme Activity Measurements**

| LDH | total volume of reaction solution | added | nanozyme concentration(mg/mL) | $b_{nanozyme}$ (IU) | $a_{nanozyme}$ (IU·mg$^{-1}$) |
|---|---|---|---|---|---|
| MgAl−$Cl^-$ | 2500 $\mu$L | 500 $\mu$L | 0.1 | 0.02 | 0.40 |
| MgAl−$CO_3^{2-}$ | | | | 0.028 | 0.56 |
| MgAl−$NO_3^-$ | | | | 0.013 | 0.26 |
| MgAl−$SO_4^{2-}$ | | | | 0.019 | 0.38 |
| CoAl | | | | 0.028 | 0.56 |
| NiAl | | | | 0.01 | 0.20 |
| NiFe | | | | 0.016 | 0.32 |
| FeAl | | | | 0.013 | 0.26 |

concentration range. Fitting the data with the Michaelis−Menten model yielded the parameters shown in Tables 4 and 5. In a study of the main enzyme kinetic parameters of LDHs ($K_m$ and $V_{max}$), the $V_{max}$ value was related to the catalytic rate, and the $K_m$ value characterized the affinity of the catalyst for the substrate. In general, $K_m$ is a measure of the binding ability of the enzyme to the substrate. The smaller the $K_m$ value is, the stronger the binding ability of the enzyme to the substrate, and the stronger the affinity is, the higher the catalytic efficiency; the greater the $K_m$ value is, the weaker the affinity and the lower the catalytic efficiency.[4,42] As indicated in Tables 4 and 5, the kinetic parameters showed that the LDHs had stronger affinities for $H_2O_2$, and the $K_m$ values for TMB were approximately 1000 times those for $H_2O_2$. Among the samples


https://doi.org/10.1021/acsomega.3c03287
ACS Omega 2023, 8, 35779−35790

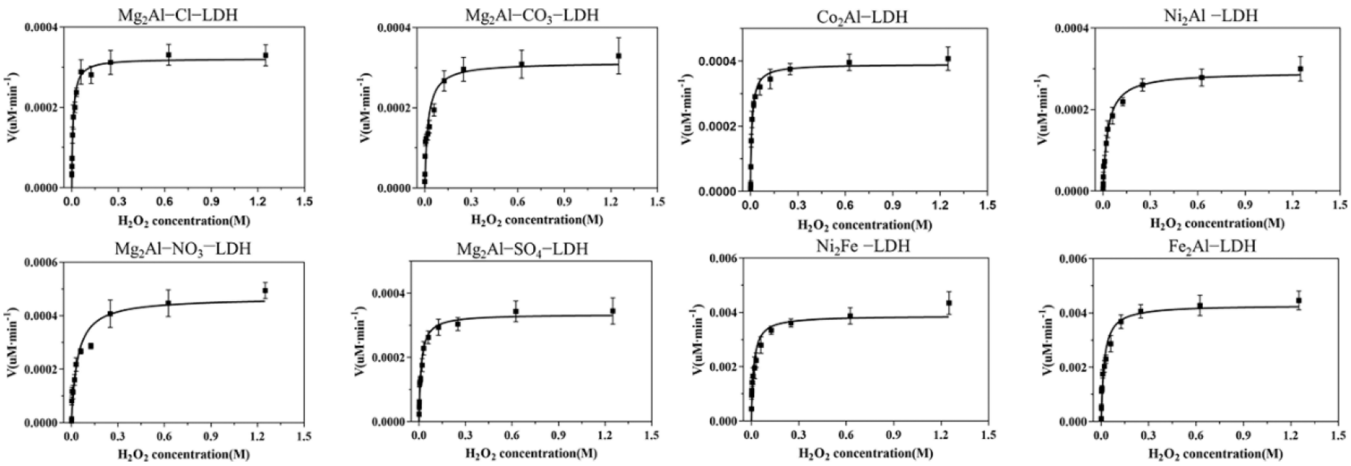


**Figure 9.** Characterization of the catalytic kinetics of peroxidase nanozymes. Michaelis−Menten curves for LDHs. The concentration of TMB used was 1.6 M, and the $H_2O_2$ concentration varied from 0 to 1.25 mM (the error bars shown represent the standard error derived from three independent experiments; $v$ is the initial reaction velocity).

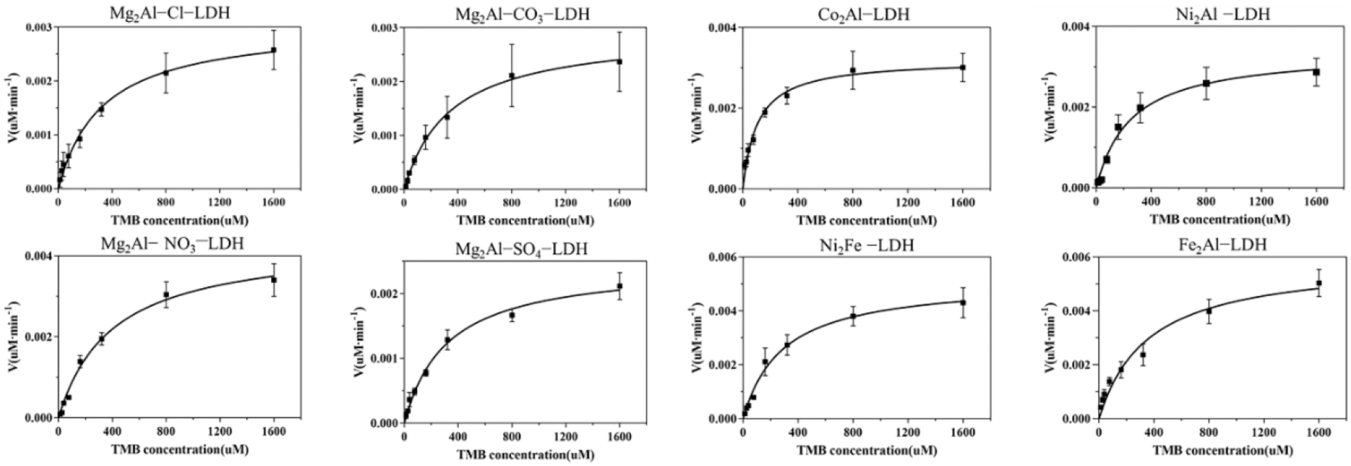


**Figure 10.** Characterization of the catalytic kinetics of peroxidase nanozymes. Michaelis−Menten curves for the prepared LDHs. The concentration of $H_2O_2$ used was 1 M, and the TMB concentration varied from 0.0128 to 1.6 mM (the error bars shown represent the standard error derived from three independent experiments; $v$ is the initial reaction velocity).

**Table 4. $K_m$ and $V_{max}$ with $H_2O_2$ as the Substrate of the LDHs with Different Anions and Cations**

| LDH | $K_m$ (mM) | $V_{max}$ (M $s^{-1}$) |
|---|---|---|
| MgAl−$Cl^-$ | $3.35 \times 10^{-4}$ | $1.35 \times 10^{-2}$ |
| MgAl−$CO_3^{2-}$ | $3.43 \times 10^{-4}$ | $3.43 \times 10^{-2}$ |
| MgAl−$NO_3^-$ | $6.06 \times 10^{-4}$ | $7.35 \times 10^{-2}$ |
| MgAl−$SO_4^{2-}$ | $3.66 \times 10^{-4}$ | $2.00 \times 10^{-2}$ |
| CoAl | $4.10 \times 10^{-4}$ | $1.24 \times 10^{-2}$ |
| NiAl | $3.24 \times 10^{-4}$ | $3.86 \times 10^{-2}$ |
| NiFe | $3.78 \times 10^{-3}$ | $1.52 \times 10^{-1}$ |
| FeAl | $4.61 \times 10^{-3}$ | $2.84 \times 10^{-1}$ |

**Table 5. $K_m$ and $V_{max}$ with TMB as the Substrate of the LDHs with Different Anions and Cations**

| LDHs | $K_m$ (mM) | $V_{max}$ (M $s^{-1}$) |
|---|---|---|
| MgAl−$Cl^-$ | 329 | $3.06 \times 10^{-3}$ |
| MgAl−$CO_3^{2-}$ | 348 | $2.93 \times 10^{-3}$ |
| MgAl−$NO_3^-$ | 398 | $4.37 \times 10^{-3}$ |
| MgAl−$SO_4^{2-}$ | 316 | $2.46 \times 10^{-3}$ |
| CoAl | 106 | $3.21 \times 10^{-3}$ |
| NiAl | 252 | $3.39 \times 10^{-3}$ |
| NiFe | 287 | $5.14 \times 10^{-3}$ |
| FeAl | 357 | $5.91 \times 10^{-3}$ |

with different anions, $Mg_2Al$-Cl-LDH had a stronger affinity for $H_2O_2$, and $Mg_2Al$-$SO_4$-LDH had a stronger affinity for TMB than did the other LDHs. With various cations, CoAl-LDH had a stronger affinity for $H_2O_2$ and TMB. With $H_2O_2$ as the substrate of the LDHs with different anions and cations, the $V_{max}$ value of $Mg_2Al$-$NO_3$-LDH was 2 times higher than those of other LDHs, the $V_{max}$ values of NiFe-LDH and FeAl-LDH were 10 times higher than those of the other LDHs, and the peroxidase-like activity of the LDHs intercalated with different anions was in the following order: $Mg_2Al$-$NO_3$-LDHs > $Mg_2Al$-$CO_3$-LDHs> $Mg_2Al$-$SO_4$-LDH > $Mg_2Al$-Cl-LDHs. The order of peroxidase-like activity of the LDHs with different cations was $Fe_2Al$-LDHs > $Ni_2Fe$-LDHs > $Ni_2Al$-LDHs > $Co_2Al$-LDHs.

**3.5. Enzymatic Reaction Kinetics of LDHs.** There have been many reports of peroxidasemics, and the typical species are $Fe_3O_4$ and AuNPs. These species react with $H_2O_2$ through the Fenton process to form hydroxyl radicals ($HO^{\cdot}$), which can oxidize the TMB substrate and thus exhibit peroxidase activity. However, some studies have shown that $HO^{\cdot}$ can be produced


https://doi.org/10.1021/acsomega.3c03287
ACS Omega 2023, 8, 35779−35790

not only by the Fenton reaction but also by releasing $Fe^{3+}$. When the LDHs with four different anions and the same shape reacted with $H_2O_2$ as the substrate, the $V_{max}$ value of $Mg_2Al$-$NO_3$-LDH was 2 times higher than those of other LDHs; this may be because from a microscale point of view, the catalytic activities of nanoparticles are determined by the total number of catalytically active sites and the activity of each site,[37] and smaller nanoparticles have larger surface active areas and lower $H_2O_2$ reduction potentials for interaction with the substrate, greatly contributing to their catalytic performance.[2] The peroxidase-like activity of LDHs with different anions was small and not very different when the specific surface area was similar. A possible reason for this finding is that these anions had an inhibitory effect on the peroxidase of LDHs.[43] In the LDHs with different cations, when the shapes and sizes were similar, the $V_{max}$ values of NiFe-LDH and FeAl-LDH were 10 times higher than those of the other LDHs, which may have been due to the presence of $Fe^{2+}$ and $Fe^{3+}$ in the NiFe-LDH and FeAl-LDH nanoparticles.[44] A possible reason for the higher peroxidase activity of FeAl-LDH than of NiFe-LDH is the electron-transfer mechanism. The $Fe^{3+}$ ions in FeAl-LDH first oxidized TMB by scraping an electron in TMB[7], and $Fe^{3+}$ was reduced to $Fe^{2+}$. Hydrogen peroxide was then decomposed into $HO^{\cdot}$ using $Fe^{2+}$ as a catalyst. At the same time, $Fe^{2+}$ was oxidized back to $Fe^{3+}$. The volcano plot of $HO^{\cdot}$ can be used to explain the structure−activity relationship of FeAl-LDH in principle. It was assumed that the exact atomic structure of the catalytic center is known; the higher the content of $Fe^{2+}$ is, the stronger the chemical reduction on the surface and thus the stronger the affinity for the hydroxyl groups.[45]

These results also indicate that the presence of $Fe^{2+}$ and $Fe^{3+}$ in the LDHs had a much greater effect on the peroxidase activity than on the particle size. NiFe-LDH and FeAl-LDH had high peroxidase activity. Compared with those of $Fe_3O_4$ and Au,[42] their $V_{max}$ values were 1000 times, and they had high catalytic activity for $H_2O_2$ and TMB and provided more alternatives to natural enzymes.

## 4. CONCLUSIONS

In this study, LDHs with four different cations and four different anions were prepared by a coprecipitation-hydrothermal method. The peroxidase-like activities and catalytic kinetics of the different anionic and cationic LDHs were studied. This study provides new insights into the application of the peroxidase activity in biosensors. When $Fe^{2+}$ or $Fe^{3+}$ was present on an LDH, this LDH maintained higher catalytic activity, showing a wider functional range than HRP or other peroxidases. These results also showed that the presence of $Fe^{2+}$ and $Fe^{3+}$ had a greater effect on the peroxidase activity of LDHs than on the particle size. These preliminary findings are the first step toward the substitution of LDH for enzymes, and these materials are expected to be applied in in vivo studies as intracellular enzymes in the future.

## ■ ASSOCIATED CONTENT

### Supporting Information

The Supporting Information is available free of charge at https://pubs.acs.org/doi/10.1021/acsomega.3c03287.

Details of LDH peroxidase-like activity data (PDF)

## ■ AUTHOR INFORMATION


### Corresponding Author

**Feng Shi** − *College of Life Science, Shihezi University, Shihezi, Xinjiang 832003, P. R. China;* orcid.org/0000-0002-2407-1239; Email: shifeng2314@yeah.net

### Authors

**MingZe Ma** − *College of Life Science, Shihezi University, Shihezi, Xinjiang 832003, P. R. China*

**Hai Wang** − *College of Life Science, Shihezi University, Shihezi, Xinjiang 832003, P. R. China*

**TieYing Zhang** − *College of Life Science, Shihezi University, Shihezi, Xinjiang 832003, P. R. China*

**XueJing Wang** − *College of Life Science, Shihezi University, Shihezi, Xinjiang 832003, P. R. China*

**ZhiHua Xu** − *College of Life Science, Shihezi University, Shihezi, Xinjiang 832003, P. R. China*

**RenYin Zhang** − *College of Life Science, Shihezi University, Shihezi, Xinjiang 832003, P. R. China*

**XiaoYu Ma** − *College of Life Science, Shihezi University, Shihezi, Xinjiang 832003, P. R. China*

Complete contact information is available at: https://pubs.acs.org/10.1021/acsomega.3c03287


### Author Contributions

F.S. provided the experimental platform, M.M. conducted the preparation of the LDHs and drafted the initial manuscript. H.W. and X.W. carried out the analysis and interpretation of data. T.Z. and X.M. participated in the design of the study and performed the statistical analysis. Z.X. and R.Z. conceived of the study, participated in its design and coordination, and helped to draft the manuscript and revise the manuscript for important intellectual content. All authors read and approved the final manuscript. The manuscript was written through contributions of all authors. All authors have given approval to the final version of the manuscript.


### Funding

This research was supported by the National Natural Science Foundation of China (32060224) and the Innovative Development Project of Shihezi University (CXFZ202110).


### Notes

The authors declare no competing financial interest.


## ■ ACKNOWLEDGMENTS

F.S. acknowledges the support from the National Natural Science Foundation of China (32060224) and the Innovative Development Project of Shihezi University (CXFZ202110).


## ■ REFERENCES


(1) Zuo, H.; Chen, W.; Cooper, H. M.; Xu, Z. P. A Facile Way of Modifying Layered Double Hydroxide Nanoparticles with Targeting Ligand-Conjugated Albumin for Enhanced Delivery to Brain Tumour Cells. *ACS Appl. Mater. Interfaces* **2017**, *9* (24), 20444−20453.

(2) Gao, L.; Zhuang, J.; Nie, L.; Zhang, J.; Zhang, Y.; Gu, N.; Wang, T.; Feng, J.; Yang, D.; Perrett, S.; et al. Intrinsic peroxidase-like activity of ferromagnetic nanoparticles. *Nat. Nanotechnol.* **2007**, *2* (9), 577−583.

(3) Wei, H.; Wang, E. Nanomaterials with enzyme-like characteristics (nanozymes): next-generation artificial enzymes. *Chem. Soc. Rev.* **2013**, *42* (14), 6060−6093.

(4) Zhang, R.; Fan, K.; Yan, X. Nanozymes: created by learning from nature. *Sci. China Life Sci.* **2020**, *63* (8), 1183−1200.

(5) Wu, J.; Wang, X.; Wang, Q.; Lou, Z.; Li, S.; Zhu, Y.; Qin, L.; Wei, H. Nanomaterials with enzyme-like characteristics (nanozymes): next-generation artificial enzymes (II). *Chem. Soc. Rev.* **2019**, *48* (4), 1004−1076.
(6) Tian, Z. M.; Li, J.; Zhang, Z. Y.; Gao, W.; Zhou, X. M.; Qu, Y. Q. Highly sensitive and robust peroxidase-like activity of porous nanorods of ceria and their application for breast cancer detection. *Biomaterials* **2015**, *59*, 116−124.
(7) Dong, J. L.; Song, L. N.; Yin, J. J.; He, W. W.; Wu, Y. H.; Gu, N.; Zhang, Y. $Co_3O_4$ Nanoparticles with Multi-Enzyme Activities and Their Application in Immunohistochemical Assay. *ACS Appl. Mater. Interfaces* **2014**, *6* (3), 1959−1970.
(8) Shen, X. M.; Wang, Z. Z.; Gao, X. F.; Zhao, Y. L. Density Functional Theory-Based Method to Predict the Activities of Nanomaterials as Peroxidase Mimics. *ACS Catal.* **2020**, *10* (21), 12657−12665.
(9) Fan, G.; Li, F.; Evans, D. G.; Duan, X. Catalytic applications of layered double hydroxides: recent advances and perspectives. *Chem. Soc. Rev.* **2014**, *43* (20), 7040−7066.
(10) Wang, Q.; O'Hare, D. Recent advances in the synthesis and application of layered double hydroxide (LDH) nanosheets. *Chem. Rev.* **2012**, *112* (7), 4124−4155.
(11) Liu, Y.; Wang, N.; Pan, J. H.; Steinbach, F.; Caro, J. In situ synthesis of MOF membranes on ZnAl-$CO_3$ LDH buffer layer-modified substrates. *J. Am. Chem. Soc.* **2014**, *136* (41), 14353−14356.
(12) Wu, Y.; Lazic, P.; Hautier, G.; Persson, K.; Ceder, G. First principles high throughput screening of oxynitrides for water-splitting photocatalysts. *Energy Environ. Sci.* **2013**, *6* (1), 157−168.
(13) Goh, K. H.; Lim, T. T. Influences of co-existing species on the sorption of toxic oxyanions from aqueous solution by nanocrystalline Mg/Al layered double hydroxide. *J. Hazard. Mater.* **2010**, *180* (1−3), 401−408.
(14) Jouyban, A.; Amini, R. Layered double hydroxides as an efficient nanozyme for analytical applications. *Microchem. J.* **2021**, *164*, No. 105970.
(15) Amini, R.; Asadpour-Zeynali, K. Layered double hydroxide nanoparticles embedded in a biopolymer: a novel platform for electroanalytical determination of diazepam. *New J. Chem.* **2019**, *43* (19), 7463−7470.
(16) Elgendy, A.; El Basiony, N. M.; El-Taib Heakal, F.; Elkholy, A. E. Mesoporous Ni-Zn-Fe layered double hydroxide as an efficient binder-free electrode active material for high-performance supercapacitors. *J. Power Sources* **2020**, *466*, No. 228294.
(17) Xu, M.; Wei, M. Layered Double Hydroxide-Based Catalysts: Recent Advances in Preparation, Structure, and Applications. *Adv. Funct. Mater.* **2018**, *28* (47), No. 1802943.
(18) Yan, L.; Gonca, S.; Zhu, G.; Zhang, W.; Chen, X. Layered double hydroxide nanostructures and nanocomposites for biomedical applications. *J. Mater. Chem. B* **2019**, *7* (37), 5583−5601.
(19) Xu, J.; Tan, Q.; Mei, Y. Corrosion protection of steel by Mg-Al layered double hydroxides in simulated concrete pore solution: Effect of $SO_4^{2-}$. *Corros. Sci.* **2020**, *163*, No. 108223.
(20) Xu, Z. P.; Stevenson, G.; Lu, C. Q.; Lu, G. Q. Dispersion and size control of layered double hydroxide nanoparticles in aqueous solutions. *J. Phys. Chem. B* **2006**, *110* (34), 16923−16929.
(21) Dong, H.; Chen, M.; Rahman, S.; Parekh, H. S.; Cooper, H. M.; Xu, Z. P. Engineering small MgAl-layered double hydroxide nanoparticles for enhanced gene delivery. *Appl. Clay Sci.* **2014**, *100*, 66−75.
(22) Xu, Z. P.; Stevenson, G. S.; Lu, C. Q.; Lu, G. Q.; Bartlett, P. F.; Gray, P. P. Stable suspension of layered double hydroxide nanoparticles in aqueous solution. *J. Am. Chem. Soc.* **2006**, *128* (1), 36−37.
(23) Peng, W.; Li, H.; Song, S. Synthesis of Fluorinated Graphene/CoAl-Layered Double Hydroxide Composites as Electrode Materials for Supercapacitors. *ACS Appl. Mater. Interfaces* **2017**, *9* (6), 5204−5212.
(24) Xiaoliang, F.; Cao, Q.; Meng, F.; Song, B.; Bai, Z.; Zhao, Y.; Chen, D.; Zhou, Y.; Song, M. A Fenton-like system of biochar loading Fe-Al layered double hydroxides (FeAl-LDH@BC)/$H_2O_2$ for phenol removal. *Chemosphere* **2021**, *266*, No. 128992.
(25) Piccinni, M.; Bellani, S.; Bianca, G.; Bonaccorso, F. Nickel-Iron Layered Double Hydroxide Dispersions in Ethanol Stabilized by Acetate Anions. *Inorg. Chem.* **2022**, *61* (11), 4598−4608.
(26) Yang, W.; Gao, Z.; Wang, J.; Ma, J.; Zhang, M.; Liu, L. Solvothermal one-step synthesis of Ni-Al layered double hydroxide/carbon nanotube/reduced graphene oxide sheet ternary nanocomposite with ultrahigh capacitance for supercapacitors. *ACS Appl. Mater. Interfaces* **2013**, *5* (12), 5443−5454.
(27) Rosa, M.; Costa Bassetto, V.; Girault, H. H.; Lesch, A.; Esposito, V. Assembling Ni−Fe Layered Double Hydroxide 2D Thin Films for Oxygen Evolution Electrodes. *ACS Appl. Energy Mater.* **2020**, *3* (1), 1017−1026.
(28) Wang, K.; Zhang, L.; Su, Y.; Shao, D.; Zeng, S.; Wang, W. Photoreduction of carbon dioxide of atmospheric concentration to methane with water over CoAl-layered double hydroxide nanosheets. *J. Mater. Chem. A* **2018**, *6* (18), 8366−8373.
(29) Wu, Y.; Gu, W.; Chen, C.; Do, S. T.; Xu, Z. P. Optimization of Formulations Consisting of Layered Double Hydroxide Nanoparticles and Small Interfering RNA for Efficient Knockdown of the Target Gene. *ACS Omega* **2018**, *3* (5), 4871−4877.
(30) Bugnicourt, L.; Ladaviere, C. A close collaboration of chitosan with lipid colloidal carriers for drug delivery applications. *J. Controlled Release* **2017**, *256*, 121−140.
(31) Xu, Z. P.; Stevenson, G.; Lu, C. Q.; Lu, G. Q. Dispersion and size control of layered double hydroxide nanoparticles in aqueous solutions. *J. Phys. Chem. B* **2006**, *110* (34), 16923−16929.
(32) Sencadas, V.; Correia, D. M.; Ribeiro, C.; Moreira, S.; Botelho, G.; Ribelles, J. L. G.; Lanceros-Mendez, S. Physical-chemical properties of cross-linked chitosan electrospun fiber mats. *Polym. Test.* **2012**, *31* (8), 1062−1069.
(33) Xu, Z. P.; Zeng, H. C. Abrupt Structural Transformation in Hydrotalcite-like Compounds $Mg_{1-x}Al_x(OH)_2(NO_3)_x{\cdot}nH_2O$ as a Continuous Function of Nitrate Anions. *J. Phys. Chem. B* **2001**, *105* (9), 1743−1749.
(34) Chakraborti, M.; Jackson, J. K.; Plackett, D.; Brunette, D. M.; Burt, H. M. Drug intercalation in layered double hydroxide clay: application in the development of a nanocomposite film for guided tissue regeneration. *Int. J. Pharm.* **2011**, *416* (1), 305−313.
(35) Li, T.; Hu, P.; Li, J.; Huang, P.; Tong, W.; Gao, C. Enhanced peroxidase-like activity of Fe@PCN-224 nanoparticles and their applications for detection of $H_2O_2$ and glucose. *Colloids Surf., A* **2019**, *577*, 456−463.
(36) ((36)) Liu, X.; Mei, X.; Yang, J.; Li, Y. Hydrogel-Involved Colorimetric Platforms Based on Layered Double Oxide Nanozymes for Point-of-Care Detection of Liver-Related Biomarkers. *ACS Appl. Mater. Interfaces* **2022**, *14* (5), 6985−6993.
(37) Greeley, J.; Stephens, I. E. L.; Bondarenko, A. S.; Johansson, T. P.; Hansen, H. A.; Jaramillo, T. F.; Rossmeisl, J.; Chorkendorff, I.; Norskov, J. K. Alloys of platinum and early transition metals as oxygen reduction electrocatalysts. *Nat. Chem.* **2009**, *1* (7), 552−556.
(38) Jv, Y.; Li, B.; Cao, R. Positively-charged gold nanoparticles as peroxidase mimic and their application in hydrogen peroxide and glucose detection. *Chem. Commun.* **2010**, *46* (42), 8017−8019.
(39) Jiang, D.; Ni, D.; Rosenkrans, Z. T.; Huang, P.; Yan, X.; Cai, W. Nanozyme: new horizons for responsive biomedical applications. *Chem. Soc. Rev.* **2019**, *48* (14), 3683−3704.
(40) Perez-Benito, J. F. Iron(III)−Hydrogen Peroxide Reaction: Kinetic Evidence of a Hydroxyl-Mediated Chain Mechanism. *J. Phys. Chem. A* **2004**, *108* (22), 4853−4858.
(41) Warkhade, S. K.; Singh, R. P.; Das, R. S.; Gaikwad, G. S.; Zodape, S. P.; Pratap, U. R.; Maldhure, A.; Wankhade, A. V. $CoSe_2$ nanoflakes: An artificial nanoenzyme with excellent peroxidase like activity. *Inorg. Chem. Commun.* **2021**, *126*, No. 108461.
(42) Jiang, B.; Duan, D.; Gao, L.; Zhou, M.; Fan, K.; Tang, Y.; Xi, J.; Bi, Y.; Tong, Z.; Gao, G. F.; et al. Standardized assays for determining the catalytic activity and kinetics of peroxidase-like nanozymes. *Nat. Protoc.* **2018**, *13* (7), 1506−1520.

(43) Sharifi, H.; Tashkhourian, J.; Hemmateenejad, B. An array of metallic nanozymes can discriminate and detect a large number of anions. *Sens. Actuators, B* **2021**, *339*, No. 129911.
(44) Dutta, A. K.; Maji, S. K.; Srivastava, D. N.; Mondal, A.; Biswas, P.; Paul, P.; Adhikary, B. Synthesis of FeS and FeSe nanoparticles from a single source precursor: a study of their photocatalytic activity, peroxidase-like behavior, and electrochemical sensing of $H_2O_2$. *ACS Appl. Mater. Interfaces* **2012**, *4* (4), 1919−1927.
(45) Shen, X. M.; Wang, Z. Z.; Gao, X. J. J.; Gao, X. F. Reaction Mechanisms and Kinetics of Nanozymes: Insights from Theory and Computation. *Adv. Mater.* **2023**, No. 2211151, DOI: 10.1002/adma.202211151.


https://doi.org/10.1021/acsomega.3c03287
*ACS Omega* 2023, 8, 35779−35790